

**Layer-resolved imaging of magnetic interlayer coupling by domain-wall stray fields**

W. Kuch, L. I. Chelaru, K. Fukumoto, F. Porrati, F. Offi,\* M. Kotsugi, and J. Kirschner

*Max-Planck-Institut für Mikrostrukturphysik, Weinberg 2, D-06120 Halle, Germany*

(Received 22 October 2002; revised manuscript received 3 February 2003; published 4 June 2003)

Layer-resolved magnetic domain images of epitaxially grown Co/Cu/Ni trilayers on Cu(001) have been studied, taken by photoelectron emission microscopy using x-ray magnetic circular dichroism as a magnetic contrast mechanism. In these trilayers the Ni layers are magnetized perpendicularly to the film plane, whereas the Co magnetization is in the film plane. Comparison of the as-grown magnetic domain images of the Co and Ni layers reveals the influence of the magnetostatic stray fields from Ni domain walls on the Co domain pattern as a lateral displacement of the Co domain wall position compared to the Ni domain walls. The effect is quantified by comparing to the effect of external magnetic fields, and is found to be equivalent to about 250 Oe. Micromagnetic simulations using the Landau-Lifshitz-Gilbert equation confirm that size of the Ni domain wall stray field interaction.

DOI: 10.1103/PhysRevB.67.214403

PACS number(s): 75.70.Kw, 75.70.Cn

**I. INTRODUCTION**

Besides the well studied indirect oscillatory magnetic interlayer exchange coupling,<sup>1,2</sup> micromagnetic mechanisms also lead to a coupling between magnetic layers across non-magnetic spacer layers in thin film multilayered structures. These micromagnetic effects may play a crucial role for magnetoresistive applications of reduced lateral size. They are related to microscopic properties, such as structure or morphology, but also to the purely magnetic microstructure, i.e., the magnetic domain structure. Examples of the former are the magnetostatic interlayer coupling at conformal interface roughness,<sup>3</sup> or coupling by the stray magnetic fields from the edges of submicron sized elements.<sup>4-6</sup> The latter, a coupling related to the magnetic domain structure, is mediated by magnetostatic stray fields from domain walls. Such a domain wall stray field interaction was proposed to explain the high degree of antiferromagnetic order found in as-grown weakly coupled multilayers,<sup>7</sup> which is irreversibly lost upon magnetization in an external field. The creeping loss of remanent magnetization of the magnetically hard layer in repeated magnetization cycles of the soft layer in hard/soft spin valves<sup>8</sup> has been also attributed to stray field domain wall interaction.<sup>9</sup> Domain images of the hard layer, a granular CoPtCr film, revealed an oscillatory decay of the remanent magnetization consistent with micromagnetic models of magnetostatic domain wall interaction.<sup>10</sup> A depth-selective Kerr microscopy investigation showed that the magnetization reversal of the top Fe layer in Fe/MgO/Fe(001) is influenced by the stray fields from the moving domain walls of the Fe substrate.<sup>11</sup>

Despite its obvious importance, relatively little experimental work up to now has focused on the micromagnetic interactions in magnetic interlayer coupling. This may be due to the lack of adequate techniques, which must not only provide microscopic lateral resolution, but also allow layer-selective probing of the magnetic domain structure. In this paper we present a photoelectron emission microscopy (PEEM) study of ultrathin single-crystalline Co/Cu/Ni trilayers, grown epitaxially on Cu(001). Using x-ray magnetic circular dichroism (XMCD) as a magnetic contrast mechanism,

this method is capable of layer resolved microscopic magnetic domain imaging due to the element-selectivity of the XMCD. It relies on the fact that the x-ray absorption cross section at elemental absorption maxima depends on the relative orientation of the helicity vector of the circularly polarized incoming x-rays and the magnetization direction of the sample.<sup>12</sup> In PEEM the local secondary electron yield at the sample surface is used to create a magnified image of the sample, which is proportional to the local absorption and thus to the projection of the local magnetization direction onto the light incidence direction.<sup>13</sup> This allows one to image the domain configuration of each magnetic layer separately. Conclusions about the global and the micromagnetic coupling between the Co and Ni magnetic layers can be drawn from the comparison of magnetic domain images of the Co and Ni layers at the same position.

Epitaxial Ni and Co films on Cu(001) are examples of ultrathin magnetic films that exhibit different magnetic easy axes for growth on the same substrate: Whereas Co films are always magnetized in the film plane,<sup>14-16</sup> Ni films show a perpendicular magnetization over an extended thickness range.<sup>17-20</sup> This leads to a noncollinear magnetic configuration in Co/Cu/Ni trilayers on Cu(001) in the case of weak exchange coupling across the Cu layer.<sup>21</sup> The Ni magnetization points along a canted direction out of the film plane, within 45° from the surface normal, whereas the Co layer is magnetized in the film plane. Alternatingly up and down magnetized stripelike domains are formed in the Ni layer. This leads to a partial flux closure outside the Ni layer, and reduces the otherwise unfavorable magnetostatic dipolar energy of perpendicularly magnetized films. Close to the walls between these domains the flux closure lines outside the Ni layer provide a substantial magnetic field component in the film plane, in the direction perpendicular to the domain wall, as schematically shown in Fig. 1. We present layer resolved domain images of the Co/Cu/Ni trilayers which show that these stray fields from Ni domain walls strongly influence the Co domain structure in the as-grown state. By application of a competing external magnetic field we can estimate the strength of this coupling due to domain wall stray fields to about 250 Oe. This experimental result is backed up by mi-

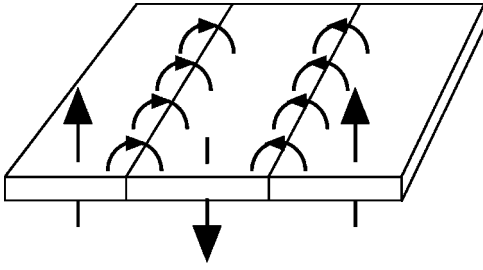


FIG. 1. Sketch of the magnetic stray field above a perpendicularly magnetized film with stripe domains. Close to the domain walls the flux closure lines provide a magnetic field component in the film plane perpendicular to the domain wall.

chromagnetic calculations, which show that, although the maximum in-plane component of the stray field from the Ni domain walls is more than 480 Oe at the position of the Co layer, the coupling effect is reduced because of the larger exchange length of the Co layer compared to the lateral extension of the stray field.

## II. EXPERIMENT

Co/Cu/Ni trilayers were grown on Cu(001) by electron bombardment from high-purity materials, and imaged at room temperature in zero field under ultrahigh vacuum conditions (base pressure  $1 \times 10^{-8}$  Pa). After deposition of the Ni layer the sample was annealed for 15 min at 450 K to reduce the interface roughness.<sup>22</sup> Cu was prepared either as a flat film or as a wedge of 150- $\mu\text{m}$  width by positioning a  $2 \times 0.5\text{-mm}^2$  slit aperture in front of the sample and rocking the sample/mask assembly about the long axis of the aperture during film deposition, as described in Ref. 23. Deposition rates were around 0.5 atomic monolayers (ML) per minute. Film thicknesses were derived from medium energy electron diffraction oscillations during growth and Auger electron spectroscopy. The systematic error in the cited thicknesses is smaller than 10% for Ni and Co, and smaller than 20% for Cu; however, the accuracy of the relative thicknesses within the wedges is about 1%.

The PEEM measurements were performed at the helical undulator beamline UE56/2-PGM2 of BESSY II in Berlin. Circularly polarized light with a degree of polarization of about 80% was incident on the sample at a  $60^\circ$  angle measured from the surface normal. The setup of the electrostatic photoelectron emission microscope (Focus IS-PEEM) is identical to that described in previous publications.<sup>24</sup> In short, it consists of an electrostatic straight optical axis microscope with an integral sample stage and a variable contrast aperture. The magnified image is intensified by a two-stage microchannel plate, and converted into visible light by means of a scintillator crystal. The image is then computer-recorded with 12-bit resolution by a Peltier-cooled camera (PCO SensiCam), which was operated with  $2 \times 2$  binning of pixels. Parameters were set to result in a lateral resolution of 350 nm and fields of view of 55 or 85  $\mu\text{m}$ . The acquisition times for the images presented here were 4 min for each helicity. Images are presented in the form of grayscale coded

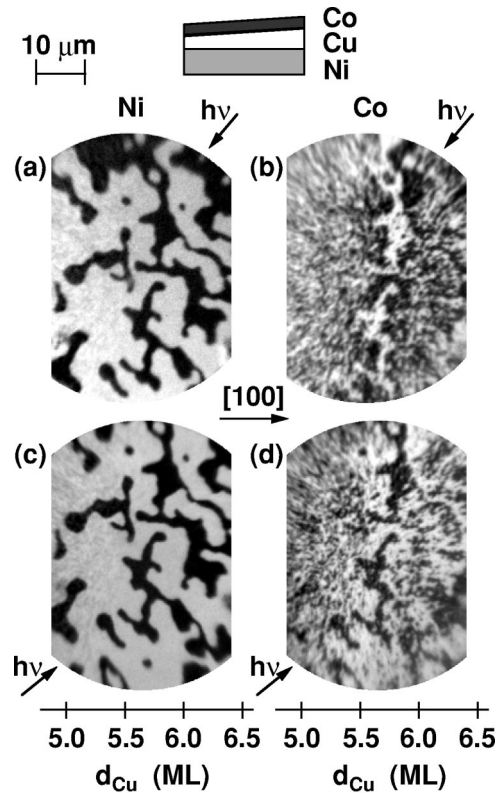


FIG. 2. Element resolved domain images of an as-grown 4-ML Co/Cu wedge/15-ML Ni/Cu(001) trilayer, the geometry of which is sketched at the top. (a) and (c) Domain images of the Ni layer. (b) and (d) Domain images of the Co layer. The Cu spacer layer thickness is indicated at the bottom axes. (a) and (b) show the layer-resolved domain patterns for a light incidence direction approximately along  $[\bar{1}\bar{1}0]$ , and (c) and (d) those for a light incidence direction approximately along  $[110]$ , as indicated by arrows labeled  $h\nu$ . A comparison of (a) and (c) and of (b) and (d) reveals that the Ni magnetization is mainly out of plane, whereas the Co magnetization is in plane.

absorption asymmetry for opposite light helicity at the maxima of the Ni and Co  $L_3$  edges, respectively.

## III. RESULTS

In Fig. 2 we present element resolved domain images of a 4-ML Co/Cu wedge/15-ML Ni/Cu(001) trilayer. The left panels (a) and (c) show domain images of the Ni layer, and panels (b) and (d) on the right show domain images of the Co layer. The sketch at the top illustrates the film structure. The Cu spacer layer thickness  $d_{Cu}$  increases from left to right between 4.9 and 6.4 ML, as indicated at the bottom axes. Panels (a) and (b) show the Ni and Co domain patterns, respectively, of the same position of the sample for a light incidence direction approximately along  $[\bar{1}\bar{1}0]$ , as indicated by arrows. In panels (c) and (d) at the bottom approximately the same area of the sample is shown for roughly opposite light incidence azimuth, also indicated by arrows. From these two sets of images the direction of the local magnetization vector in space can be determined. In particular a magnetization along the surface normal will not lead to a

change in contrast for reversal of the light incidence azimuth, whereas the contrast for a magnetization in the film plane will be reversed.

Comparing the Ni domain images (a) and (c), one recognizes that, except for the lowest Cu spacer layer thicknesses at the very left of the images, the magnetic contrast is unaffected by the light azimuth reversal. The Ni magnetization is therefore perpendicular to the film plane, where white and black correspond to magnetization pointing into the sample and out of the sample, respectively. The Ni layer exhibits the stripe/bubble pattern typical for perpendicularly magnetized films,<sup>25</sup> with domain sizes of several microns. The Co contrast, on the contrary, reverses between the domain images (b) and (d), indicating magnetization in the film plane. Here the average domain size is much smaller.

The ripple pattern in the Ni images for Cu spacer layer thicknesses of about 5 ML is correlated to the small domains in the Co layer at that position. It is a consequence of the global, large area indirect exchange coupling through the Cu spacer layer, which is stronger at lower Cu thicknesses. It leads to a canting of the Ni magnetization away from the purely perpendicular direction by tilting it into the Co in-plane magnetization direction. This is due to the competition of magnetic anisotropies of the single layers and the inter-layer coupling, and is discussed in detail in Ref. 21. The absence of this canting in the rest of the image, i.e., at higher Cu thicknesses, indicates that the exchange coupling is quite weak there.

In addition to the very different domain patterns in Ni and Co, also indications for microscopic interaction between the two layers can be found. The shapes of the bigger domains in the Co domain images [Figs. 2(b) and 2(d)] replicate the shapes of the Ni out-of-plane domains at the very same place. To study the microscopic interaction between the two magnetic layers in more detail, Fig. 3 shows a larger magnification of panels (c) and (d) of Fig. 2. The images of Fig. 3 are shown rotated by 45° with respect to Fig. 2, with the [110] direction along the horizontal of the figure. Panel (a) shows the Ni domain pattern, panel (b) the corresponding Co domain pattern. The local magnetization direction is indicated in some of the domains. The Co domains are mainly magnetized along the [110] (white) and the  $[\bar{1}\bar{1}0]$  crystallographic directions (black). The  $\langle 110 \rangle$  in-plane directions are the easy axes of Co films on Cu(001).<sup>16</sup>

White lines in the Co image [Fig. 3(b)] mark the position of Ni domain walls obtained from the 50% intermediate contour line between white and black in a contour plot of Fig. 3(a). They facilitate a discussion of the correlation between the as-grown Ni and Co domain patterns. All the larger black domains in the Co image [Fig. 3(b)] are related to similarly shaped Ni domains of Fig. 3(a). At about the middle of the image these black domains in Co correspond to black domains in Ni, whereas at the bottom of the image a black domain in Co is located at the position of a white domain in Ni.

A closer inspection of the element resolved domain patterns reveals that in regions of correlated domain patterns the domain walls in Co are shifted right or left with respect to the domain walls in Ni. Two such positions are pointed out

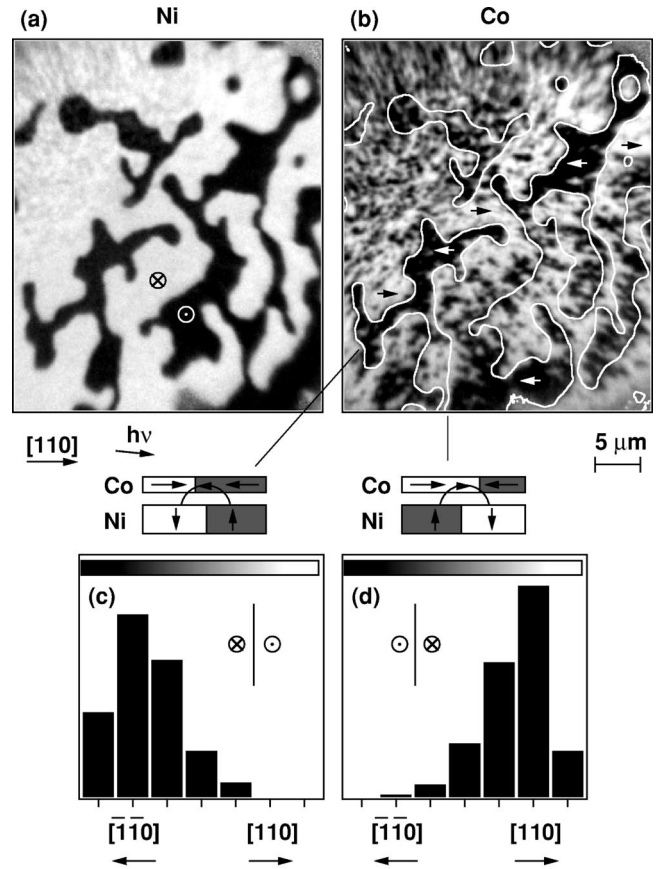


FIG. 3. Element resolved domain images of the as-grown 4-ML Co/Cu wedge/15-ML Ni/Cu(001) trilayer, corresponding to Figs. 2(c) and 2(d). (a) Domain image of the Ni layer. (b) domain image of the Co layer. The white lines in (b) mark the position of Ni domain walls in (a). Two sketches underneath the domain images illustrate the relative orientation of Ni and Co magnetization at the two indicated spots in the image. (c) Histogram of the Co magnetization contrast above Ni domain wall sections which run within  $\pm 25^\circ$  along the image vertical and correspond to the situation shown in the left sketch. (d) The same as in (c), but for Ni domain wall sections corresponding to the right sketch.

by lines at the bottom of Fig. 3(b), and the situation at these domain boundaries is illustrated by sketches below the images. The shift of the Co domain walls can be explained by stray fields from the Ni domain walls. Let us first consider the left sketch. A domain wall in Ni separates a white/down domain on the left from a black/up domain on the right. This causes a stray field above the Ni film with an in-plane component pointing to the left, as indicated in the sketch. The Co layer, at that position, has a white/right domain on the left hand side, and a black/left domain on the right hand side. Since the in-plane component of the stray field from the Ni domain wall is pointing to the left, the domain wall in Co is shifted to the left in order to expand the black/left domain on the expense of the white/right domain.

The other sketch on the right hand side illustrates a spot on the sample where the opposite situation is encountered: Here a domain wall is separating a white/right domain in Co on top of a black/up domain in Ni on the left hand side from a black/left domain in Co on top of a white/down domain in

Ni on the right hand side. The stray field above the Ni domain wall is now pointing to the right. This extends the white/right domain in Co, and leads to a shift of the Co domain wall to the right.

The effect of the Ni domain walls on the Co magnetization is also clearly observed in parts of the image where the Co domain pattern does not exactly reproduce the bigger Ni domains, for example in the right bottom quarter of the image. Here the Ni domain walls run predominantly along the vertical direction. Following the Ni domain walls in the Co image, it is clearly observed that small Co domains, either black or white, chain up along these Ni domain walls.

A statistical analysis of the whole image range is presented as histogram plots in Figs. 3(c) and 3(d). Since the light incidence is from the left, the contrast in the Co image is sensitive to the component of the in-plane magnetization along the image horizontal. The in-plane component of the stray field points perpendicular to the domain wall; cf. Fig. 1. Domain wall stray fields along the horizontal direction are consequently caused by Ni domain walls running along the vertical direction of Fig. 3. The Co contrast found above vertical sections of Ni domain walls has been statistically analyzed, and its distribution is presented in the form of histogram plots in panels (c) and (d). Here the meaning of “vertical” was extended to include Ni domain wall sections that are inclined by up to  $\pm 25^\circ$  from the vertical direction. In this way the analysis for each of the two histogram plots includes a total Ni domain wall length of  $100 \mu\text{m}$ . Compared to the average Co domain size of about  $2 \mu\text{m}$ , the number of evaluated Co domains is about 50 for each histogram plot. Including Ni domain wall sections that are inclined up to  $\pm 60^\circ$  from the vertical direction does not lead to a qualitative change of the histograms. Figure 3(c) shows the histogram corresponding to the situation of the left sketch, where a Ni domain wall separates a white/down domain on the left from a black/up domain on the right. Figure 3(d) shows the histogram corresponding to the situation of the right sketch. The grayscale bars at the top of panels (c) and (d) indicate the graytones of Fig. 3(b) which correspond to the respective histogram bars.

It is clearly seen that in the Co layer virtually everywhere above close-to-vertical Ni domain walls the magnetic contrast in Co is either black or white, i.e., pointing to the left or right, depending on the direction of the stray field from the Ni domain wall. This minimizes the Zeeman energy of the Co magnetization in the local stray field of the Ni domain wall.

To get an estimate of the size of the stray fields from the Ni domain walls in the Co layer, the effect of an external magnetic field on the Co domain pattern in Co/Cu/Ni/Cu(001) was studied. Figure 4 shows the effect of an external magnetic field on element resolved remanent domain images. Here the sample was a 4-ML Co/6-ML Cu/15.5-ML Ni trilayer on Cu(001), and the magnetic field was applied by pulses of about 1 ms duration in between subsequent exposures. The field of view was selected to have Ni domain walls running predominantly in one direction, here roughly along  $[120]$ . Frames (a) and (b) show the as-grown domain patterns of the Ni and Co layer, respectively. The light inci-

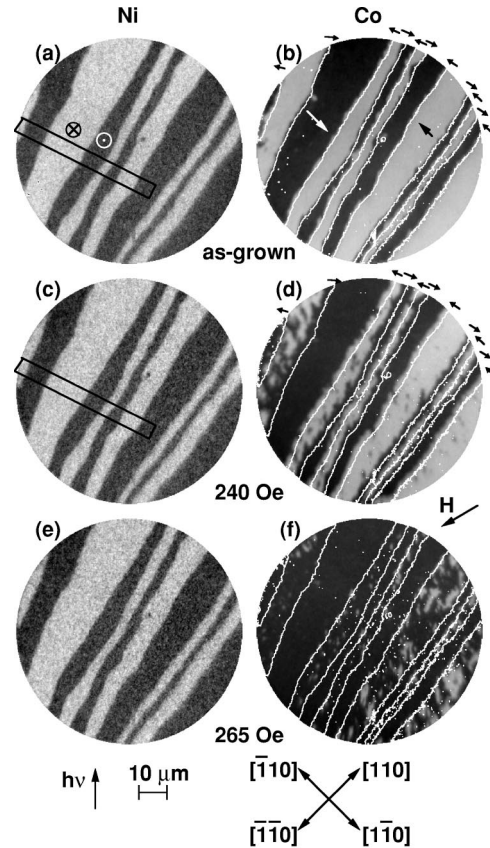


FIG. 4. Element resolved domain images of a 4-ML Co/6-ML Cu/15.5-ML Ni trilayer on Cu(001). (a), (c), and (e) Ni domain patterns; (b), (d), and (f) Co domain patterns. (a) and (b) show the domain patterns of the as-grown trilayer; (c) and (d) after the application of a 240-Oe external field in the direction labeled by “H”; (e) and (f) after the application of a 265-Oe external field in the same direction. The white lines in (b), (d), and (f) mark the position of Ni domain walls in the respective Ni domain images (a), (c), and (e). The small arrows above the upper edge of (b) and (d) mark the direction of the in-plane component of the stray fields caused by the Ni domain walls. The rectangles in (a) and (c) indicate the area where the line scans presented in Fig. 5 have been taken.

dence azimuth was along  $[010]$ , as indicated at the bottom of Fig. 4. Arrows in the images indicate the direction of local magnetization. Within the field of view, in Co only  $[\bar{1}10]$  and  $[1\bar{1}0]$  domains are observed, as was confirmed by azimuthal rotation of the sample. Note that for the present geometry, where the azimuthal angle of light incidence is  $45^\circ$  to the  $[110]$  direction, the contrast from  $[110]$  and  $[\bar{1}10]$  magnetization directions would be indistinguishable, and also the contrast from  $[\bar{1}\bar{1}0]$  and  $[1\bar{1}0]$ .

Only one of the two senses of correlation between Ni and Co magnetization, the one corresponding to the left sketch in Fig. 3 and its periodic extension to a stripelike pattern, is present here. The position of Ni domain walls, obtained from a contour plot of the Ni domain pattern of Fig. 4(a), is superimposed on Fig. 4(b) as white lines. It is clearly seen that the domain walls in Co are shifted upwards and to the left compared to the Ni domain walls, similar to Fig. 3. Small

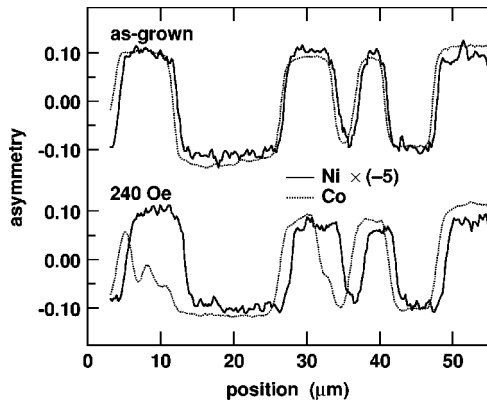


FIG. 5. Line scans of the image asymmetry of a 4-ML Co/6-ML Cu/15.5-ML Ni trilayer on Cu(001), showing the displacement of the Co in-plane domain walls with respect to the Ni out-of-plane domain walls. Top: Line scans from the as-grown domain images of Figs. 4(a) and 4(b), taken along the long side of the rectangle displayed in Fig. 4(a), averaging over the short side. Bottom: Line scans from the domain images after application of a 240-Oe external field, as presented in Figs. 4(c) and 4(d). Solid lines: Scans of the Ni domain pattern, multiplied by  $-5$ ; dotted lines: scans of the Co domain pattern.

arrows at the top of Fig. 4(b) indicate the sense of the in-plane component of the stray field of each of the Ni domain walls. Line scans of the Co and Ni  $L_3$  asymmetry along the long side of the rectangle shown in Fig. 4(a) are reproduced in the upper part of Fig. 5, in which the asymmetry was averaged along the width of the rectangle. For a better comparison with the Co line scan, the Ni asymmetry has been reversed in sign and scaled by a factor of 5. The shift of the Co in-plane domain walls with respect to the Ni domain walls is very well recognized. The domain wall displacement differs a bit at each domain wall, and on average amounts to about 400 nm.

Panels (c) and (d) of Fig. 4 show the Ni and Co element resolved domain images, respectively, after the application of an external field of 240 Oe in the direction indicated by  $H$ , which was approximately along the  $[\bar{2}\bar{1}0]$  direction. Whereas the Ni image (c) is virtually unchanged after the application of the external field, significant changes are observed in the Co image. Some black domains have nucleated within the previously white domains. Because of the direction of the magnetic field, these black domains correspond to a magnetization along  $[\bar{1}\bar{1}0]$ . The white lines in panel (d) are again the 50% contour lines of panel (c). Interestingly the shift of Co domain walls compared to the Ni domain walls is now even bigger than in the as-grown images (b) vs (a). This can be more clearly seen from linescans of Figs. 4(c) and 4(d), which are presented in the lower part of Fig. 5. Like before, these scans have been taken at the region indicated by the rectangle in Fig. 4(c). The displacement of the Co domain walls is now between 1.2 and 1.7  $\mu\text{m}$ , ignoring the leftmost stripe where many dark domains have nucleated inside the previously white stripe in the Co domain image.

It should be mentioned that the observed displacement of

the Co domain walls with respect to the Ni domain walls cannot be just the result of image instabilities. Since the Co and Ni images are taken directly one after the other, any image instability should also affect the two exposures with different helicity for the same image, and thus show up in the asymmetry image as artefactual black and white contours along the domain boundaries. This is not observed. In fact, the images were found to be extremely stable and reproducible, even after hours. Since secondary electrons of identical energy are contributing to both the Ni and Co images, the different photon energy does not have an influence on the imaging conditions.

Figures 4(e) and 4(f) show the layer resolved Ni and Co domain images, respectively, of the same position after the application of a 265-Oe external magnetic field, only 15 Oe higher than before. Again the contour plot of the Ni domain walls of panel (e) is shown superimposed on the Co domain image (f) by white lines. The Ni image (e) is still unchanged after the application of the external in-plane field, but significant changes are observed in the Co image, panel (f), with respect to panel (d). Now nearly everywhere a black contrast is observed, except for some white spots remaining at the position of the previously white stripe domains at the right hand side of the image.

This behavior enables us to estimate the size of the stray field contribution to the local coupling between Ni and Co layers close to Ni domain walls. In the vicinity of Ni domain walls separating (from upper left to lower right) white down domains from black up domains, the Co image exhibits a bright contrast after the application of a 240-Oe external field, i.e., magnetization along  $[\bar{1}10]$ . The in-plane component of the stray field from these domain walls is along  $[\bar{2}10]$ . During the 240-Oe pulse, consequently, a  $[\bar{1}10]$  domain survives, and re-expands to a certain extent after the field pulse. A 265-Oe field pulse, on the other hand, seems to annihilate these domains, so that after switching off the pulse only black contrast is observed. Although the external field is approximately parallel to the domain walls, and the local field is perpendicular to them, they are both symmetric with respect to the crystallographic axes of the system. If one neglects uniaxial magnetic anisotropies of the Co layer in the plane, one can therefore estimate the effect of the local stray field from the competition of both fields. It follows that the action of the in-plane component of the stray field from the Ni domain walls on the Co layer equals about that of an external field of 250 Oe.

#### IV. DISCUSSION

In order to verify the stray field type origin of the observed domain wall displacement, micromagnetic calculations solving the Landau-Lifshitz-Gilbert equation of motion have been carried out.<sup>26</sup> The inset of Fig. 6(a) shows a sketch of the simulated structure and the starting magnetic configuration. It consisted of a 2.55-nm-thick Ni layer, the uniaxial anisotropy of which was set to  $+0.27 \text{ MJ/m}^3$ , the positive sign meaning an easy axis of magnetization out of the film plane. This value corresponds to volume and interface anisotropies of  $+29$  and  $-77 \mu\text{eV/atom}$ , respectively, taken

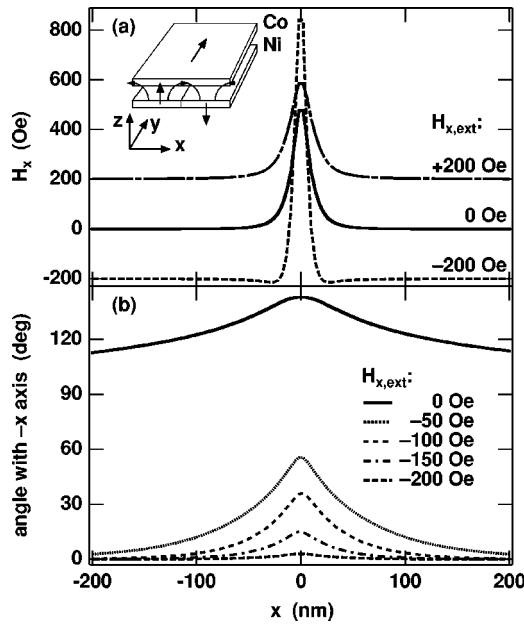


FIG. 6. Result of a micromagnetic calculation of a 0.85-nm Co/0.85-nm Cu/2.55-nm Ni trilayer with an infinitely extended periodic stripe domain structure in the Ni layer as starting configuration (see inset). (a)  $x$  component of the magnetic field at the position of the Co layer as a function of  $x$  position for three different values of external field in  $x$  direction, as indicated. (b) Azimuthal angle of the Co magnetization in the plane, measured from the  $-x$  direction, as a function of  $x$  position for five different values of external field in  $x$  direction, as indicated.

from Ref. 19, and assuming the Cu substrate areal atom density as well as  $1.70 \text{ \AA}$  vertical atomic layer separation of a 15 ML Ni film.<sup>27</sup>

A regular up and down magnetized stripe domain pattern of  $2\text{-}\mu\text{m}$  stripe width was used as starting configuration for the Ni layer, as schematically shown in the inset of Fig. 6(a). The notation is such that the stripes run perpendicular to the  $x$  direction, and are infinitely extended in the  $y$  direction.  $z$  denotes the direction along the film normal. Periodic boundary conditions in the  $x$ - $y$  plane were used for the simulations.

A 0.85-nm Co layer was placed on top of the Ni layer, separated by 0.85 nm of Cu. This corresponds to film thicknesses of 4.7 and 4.9 ML for the Cu and Co layers, respectively, using Cu bulk vertical lattice spacings and lattice parameters of Co/Cu(001) of Ref. 28. The indirect bilinear interlayer exchange coupling across the Cu spacer layer was set to  $0.25 \text{ mJ/m}^2$ , corresponding to  $100 \text{ }\mu\text{eV/atom}$ . The uniaxial anisotropy of the Co layer was chosen as  $-1.2 \text{ MJ/m}^3$  (Ref. 16). The starting configuration for the Co layer was a single-domain configuration, where all spins point into the positive  $y$  direction.

The simulation volume was discretized in square prisms of size 4 nm in the  $x$  and  $y$  directions, and 0.85 nm in the  $z$  direction. The saturation magnetization  $\mu_0 M_S$  was set to 0.60 T for Ni and 1.66 T for Co; as exchange stiffness constant  $A$  values of  $3.4 \times 10^{-12} \text{ J/m}$  for Ni and  $13 \times 10^{-12} \text{ J/m}$  for Co were used.

A slightly higher interlayer exchange coupling between

the two magnetic layers was chosen than what is expected for a 4–5-ML Cu spacer layer,<sup>21</sup> in order to study the influence of the canting of the Ni magnetization direction into the Co magnetization direction. With the above parameters the Ni magnetization is tilted by  $22^\circ$  away from the surface normal, in the direction of the Co in-plane magnetization. Experimentally such a canting corresponds to a Cu spacer layer thickness of about 3.5–4.0 ML.<sup>21</sup> The Co magnetization, on the contrary, assumes only a very small out-of-plane component because of the larger anisotropy of the Co layer.<sup>21</sup>

The domain wall stray field interaction that we want to study here induces an  $x$  component in the Co magnetization direction close to the Ni domain walls. The sketch in the inset of Fig. 6 indicates the direction of the  $x$  component of the domain wall stray field, pointing in the positive  $x$  direction at the domain wall in the center ( $x=0$ ), and in the negative ( $-x$ ) direction at the two neighboring Ni domain boundaries shown at the outside edges of the sketch ( $x = \pm 2000 \text{ nm}$ ).

After a relaxation of the starting configuration in zero external field, the Co layer was removed, and the magnetic stray field of the Ni layer was calculated at the position where the Co layer had been, without further relaxing the Ni magnetization configuration. The  $x$  component of the result is displayed in Fig. 6(a) by the solid line as a function of the  $x$  position. A sharp peak with about 20 nm full width at half maximum (FWHM) is observed. The stray field has decayed to less than 1% of its maximum value at only 54-nm distance from the center of the Ni domain wall.

The solid line in Fig. 6(b) shows the corresponding azimuthal angle of the Co magnetization direction, defined with respect to the negative  $x$  direction. The stray fields at the Ni domain walls modulate the Co magnetization about the  $+y$  direction, with an amplitude of  $\pm 53^\circ$ . This corresponds to an angle of  $90^\circ \pm 53^\circ$  with respect to the  $x$  axis. Since no anisotropy in the film plane was assumed for the simulations, this modulation is rather smooth, and the magnetization points along  $+y$  exactly only in the centers of the Ni domains, at  $x = \pm 1000 \text{ nm}$ .

The maximum value of the domain wall stray field from the simulation is 480 Oe. This is distinctly higher than the experimental estimate of 250 Oe, but much lower than the analytically calculated value for a Ni domain wall of zero thickness,<sup>29</sup> which yields nearly 2100 Oe in the center of the Co layer position, i.e., 1.28 nm above the Ni surface. Reasons for the latter discrepancy are the finite extension of the Ni domain wall (12 nm from the present simulation), and also a deviation from the ideal Bloch wall profile induced by the interlayer exchange coupling to the Co layer, as will be shown below.

The reaction of a ferromagnet on an inhomogeneous effective field which varies on a length scale comparable to or smaller than the exchange length of the magnetic material is called exchange averaging.<sup>30,31</sup> To discuss the experimentally observed domain wall coupling strength, one has to consider the effect of exchange averaging within the Co layer, which averages out some of the sharp peak of the domain wall stray field. A typical length scale for the reaction of a magnetic film on a delta-shaped field can be defined

as  $l = \sqrt{A/(H_{ext}M_S)}$ , where  $H_{ext}$  is a homogeneous external magnetic field acting against the delta field. This is demonstrated in Fig. 6(b) by including an external field in the  $-x$  direction in the simulation. The dotted and dashed lines show the in-plane angle of the Co magnetization with the external field, i.e., with the negative  $x$  axis, as a function of  $x$  position for four different values of the external field between 50 to 200 Oe. The Co magnetization deviates from the direction of the external field around  $x=0$ . The width of this deviation is clearly larger than the width of the stray field itself [cf. Fig. 6(a)]. If the external field is increased, this induced “domain” in the Co layer becomes narrower and smaller. Its FWHM follows about a  $2l$  behavior. It is finally annihilated even before it reaches the maximum of the local field. A rough estimate for this to happen is when the width of the positive part of the total field, external plus stray field, becomes narrower than the typical length  $l$ . In the simulation this is the case just above a 200-Oe external field. An experiment measuring the domain wall interaction by applying competing external fields will consequently not yield the peak value of the stray field, but the exchange averaged action on the magnetic film.

Note that  $l$  would diverge for zero external field. In the simulation this corresponds to the smooth modulation of the Co magnetization direction for zero external field. In this case only the width of the Ni stripe domains limits the extension of the resulting induced domain in the Co layer. In practice the value of  $l$  is also determined by other energy terms like fourfold or uniaxial in-plane anisotropies. Typical fourfold anisotropy fields for 4–5-ML Co/Cu(001) are of the order of 150–200 Oe,<sup>16,32</sup> comparable to the external fields used here. The presence of such anisotropies will decrease the effect of exchange averaging, so that higher external fields are needed to compensate for the influence of the local field. Considering this, the agreement between simulated annihilation of the induced domains in Co and the experiment is quite good.

An interesting point is the reaction of the Ni layer to the coupling with the Co layer. The presence of an  $x$  component of the Co magnetization at the positions of the Ni domain walls distorts the Bloch wall in the Ni. It turns out that for the chosen parameters the azimuthal angle of the in-plane component of the Ni magnetization closely follows the corresponding angle of the Co magnetization, even in the domain walls. This means that at a  $-200$ -Oe external field the Ni magnetization turns from  $+z$  to  $-x$  to  $-z$ , and not, as in a Bloch wall, from  $+z$  to  $+y$  to  $-z$  (or from  $+z$  to  $-y$  to  $-z$ ). This adds additional magnetic charge to the wall, which increases its stray field. The comparison is shown in Fig. 6(a). The two dashed and dash-dotted lines show the  $x$  component of the total magnetic field at the position of the Co layer as a function of  $x$  position for the magnetic configuration obtained by relaxing the structure with a 200-Oe external field applied in the plus and minus  $x$  directions, respectively. It is observed that the stray field from the Ni domain wall, i.e., the peak height, is indeed significantly enhanced when the in-plane magnetization inside the domain wall is pulled into  $-x$  by the interaction with the Co layer. On the other hand, if the magnetization in the wall is turning by  $+x$ ,

the stray field is reduced, because the contribution due to the in-plane magnetization in the wall and the contribution due to the out-of-plane magnetization in the domains outside the wall partially cancel each other. It has to be noted that actually the field profile for zero external field leads to a certain tilt of the wall magnetization into the positive  $x$  direction [cf. panel (b), solid line]. Therefore the maximum value of the stray field for zero external field, 480 Oe, is already influenced by partial charging of the Ni wall. In the experiment this effect will be less significant, since the interlayer exchange coupling may be less than what was assumed for the simulations, as discussed above.

The dependence of the domain wall stray field interaction on the spacer layer thickness is dominated by the rapid decrease of the stray field of an undistorted Bloch wall with vertical distance, which is nearly exponential at distances small compared to the Ni film thickness.<sup>29</sup> The additional reduction of that field from the partial charging of the wall by a turn of the magnetization component inside the wall in the positive  $x$  direction at zero external field, as discussed above, will be also weaker for higher spacer layer thicknesses. Since the turning angle depends on the in-plane angle of the Co magnetization, which is a monotonic function of the resulting stray field at the position of the Co layer, the resulting stray field will also decay monotonically with increasing spacer layer thickness. Note that small changes of the interlayer coupling strength alone would not lead to a significant change in the resulting stray field because in the range considered here this coupling aligns the in-plane component of the Ni magnetization to within a few degrees with the Co magnetization.

The experimentally observed extension of the Co domains induced by the Ni stray fields, i.e., the shift of the Co domains with respect to the Ni domains, depends on the details of the magnetization reversal mechanism in the Co layer, for example domain wall mobility and pinning, and on the energetics of all involved mechanisms, including some preferential coupling that locally links certain Co in-plane and Ni out-of-plane magnetization directions, as will be discussed below, and a possible local uniaxial in-plane anisotropy. Without a proper knowledge of the mechanism leading to the domain duplication in the Co layer and its energetics, it is not possible to simulate the observed shift of the Co domain wall boundaries with respect to the Ni domain boundaries. No attempt has therefore been made to simulate exactly the experimentally observed domain configuration of the Co layer. The larger domain shift observed after the application of the 240-Oe field pulse compared to the as-grown state (cf. Fig. 5) is an indication that the latter represents a metastable configuration. In fact the energetically most favorable remanent configuration would be a shift of the Co domains by half the stripe period of the Ni domains. It is worth noting that after application of the 240-Oe pulse [Fig. 4(d)] the Co domain configuration has come closer to this energetic minimum than in the as-grown state [Fig. 4(b)]. At some of the narrower stripe domains in Fig. 4(d) this situation seems to be indeed approximately realized.

The Ni domain wall stray field acts like a local effective field during growth of the Co layer. It will influence the critical thickness for ferromagnetic order in the Co layer, i.e., the thickness at which the ordering temperature equals room temperature. An external magnetic field suppresses magnetic fluctuations, resulting in a smaller critical thickness.<sup>33</sup> That means that during growth of the Co layer, ferromagnetic order will first be established at positions close to Ni domain walls due to the domain wall stray fields. At these positions the Co magnetization direction will be set by the direction of the stray field. It has been observed that very thin Co layers on top of 4-ML Cu/15-ML Ni/Cu(001) exhibit an out-of-plane magnetization domain pattern identical to the Ni domain pattern.<sup>34</sup> This out-of-plane magnetization of the Co layer has been attributed to the indirect exchange coupling between the Co and Ni layers and to the vanishing anisotropy of the Co layer at thicknesses below 2 ML. The Cu layer thicknesses of the trilayers presented here are slightly higher, but it is possible that also here an out-of-plane magnetization is present during the early stages of growth of the Co layer. The history of the Co magnetization during the layer deposition therefore starts from an out-of-plane domain pattern which is a replica of the Ni domain pattern, and later undergoes a spin reorientation transition to the in-plane domain pattern that is observed in the experiment after completion of the growth.

One could imagine that during that spin-reorientation transition the local magnetization may turn into any of the four equivalent  $\langle 110 \rangle$  in-plane crystallographic directions, thus losing the information about the out-of-plane domain pattern. However, in the experiment a stunning similarity between the domain patterns of the in-plane Co magnetization and the out-of-plane Ni magnetization is observed, especially in Fig. 4. Possible mechanisms leading to this domain pattern correlation may be found in the exact mechanism of the spin reorientation transition of the Co layer from out-of-plane to in-plane. In Ref. 34 no sign of branching into small domains of the out-of-plane domains towards the spin reorientation transition is observed, as is sometimes found in the vicinity of spin reorientation transitions.<sup>35,36</sup> The spin reorientation transition may therefore proceed, domain by domain, by a continuous rotation of the magnetization from out of plane to in plane. In this case it would be energetically unfavorable to create additional in-plane subdomains. Which of the four equivalent in-plane directions are assumed in each domain may then depend on subtle energy differences. Such energy differences could be due to structural details, for example preferential step edge orientation. In Fig. 3 it is in fact observed that locally the Co magnetization is rotated by the same  $90^\circ$  rotation with respect to the Ni magnetization, leading to one of the two correlation patterns schematically shown in the figure. A breaking of the fourfold substrate symmetry by a local preferential substrate step edge and terrace orientation may be a conceivable explanation. The local stray fields present at the Ni domain walls may of course also influence the Co domain pattern formed after the Co magnetization has turned to in plane. Further experimental effort is required to identify the exact mechanism responsible for this domain correlation.

The small Co domains seen in Figs. 2(b) and 2(d) and in Fig. 3(b) are absent in Fig. 4(b). Magnetic domains of two different length scales in Co/Cu(001) at different positions on the sample have been reported previously.<sup>37</sup> It is at present not clear which mechanism determines the Co domain size. Tiny differences in substrate morphology may be responsible. The absence or a reduced importance of the above discussed mechanism for domain correlation, for example a more isotropic step edge distribution, may also lead to a breaking into smaller in-plane domains of the Co magnetization.

From Fig. 4 one can see that the coercivity of the Co layer is not exactly uniform over the imaged area: From panels (d) and (f) it is clearly recognized that in both images stronger changes to the Co domain pattern occur in the upper left part of the image compared to the lower right part. Since the coils used for the external field are about 2 cm away from the sample, the nonuniformity of the field cannot be the reason for this. The coercivity is probably also influenced by details of the film and substrate morphology, which may change on a shorter length scale within the field of view.

## V. CONCLUSION

The layer resolved magnetic domain images of the Co/Cu/Ni trilayers prove the importance of the micromagnetic interaction between the two magnetic layers by magneto-static stray fields from the Ni domain walls. The apparent strength of this interaction equals a coupling field of about 250 Oe. Micromagnetic simulations support that result. They show that the peak value of the domain wall stray field can be even higher, and is leveled out to some extent by exchange averaging within the Co layer.

This result demonstrates the importance of domain wall stray field interactions for the interlayer exchange coupling. The apparent strength of the coupling may be influenced by the presence or absence of domain walls, as well as by its type. A detailed knowledge of the magnetization reversal process and the occurrence of domain walls is thus necessary to correctly describe the apparent coupling deduced from magnetization measurements of coupled systems. On the other hand, this opens a way for tailoring the effective coupling strength within the very same system by manipulating the reversal mechanism. An example is the suppression of domain wall creation by applying a transverse field during magnetization switching.

## ACKNOWLEDGMENTS

We thank B. Zada and W. Mahler for technical assistance, R. Hertel, B. Heinrich, and H. P. Oepen for stimulating discussions. Financial support by the German Federal Minister for Education and Research (BMBF) under Grant No. 05 KS1EFA6 is gratefully acknowledged.

- \*Present address: INFM, Unità Roma Tre, Via della Vasca Navale 84, I-00146 Roma, Italy.
- <sup>1</sup>*Ultrathin Magnetic Structures*, Vol. 2, edited by B. Heinrich and J. A. C. Bland (Springer, Berlin, 1994), and references therein.
  - <sup>2</sup>P. Bruno and C. Chappert, *Phys. Rev. Lett.* **67**, 1602 (1991); P. Bruno, *Phys. Rev. B* **52**, 411 (1995).
  - <sup>3</sup>L. Néel, *C. R. Hebd. Seances Acad. Sci.* **255**, 1676 (1962).
  - <sup>4</sup>X. Portier, A. K. Petford-Long, T. C. Anthony, and J. A. Brug, *J. Magn. Magn. Mater.* **187**, 145 (1998); *J. Appl. Phys.* **85**, 4120 (1999).
  - <sup>5</sup>K.-S. Moon, J. R. E. Fontana, and S. S. P. Parkin, *Appl. Phys. Lett.* **74**, 3690 (1999).
  - <sup>6</sup>T. Kimura, Y. Itagaki, F. Wakaya, and K. Gamo, *Appl. Phys. Lett.* **78**, 4007 (2001).
  - <sup>7</sup>J. A. Borchers, J. A. Dura, J. Unguris, D. Tulchinsky, M. H. Kelley, C. F. Majkrzak, S. Y. Hsu, R. Loloee, W. P. Pratt, Jr., and J. Bass, *Phys. Rev. Lett.* **82**, 2796 (1999).
  - <sup>8</sup>S. Gider, B.-U. Runge, A. C. Marley, and S. S. P. Parkin, *Science* (Washington, DC, U.S.) **281**, 797 (1998).
  - <sup>9</sup>L. Thomas, M. G. Samant, and S. S. P. Parkin, *Phys. Rev. Lett.* **84**, 1816 (2000).
  - <sup>10</sup>L. Thomas, J. Lüning, A. Scholl, F. Nolting, S. Anders, J. Stöhr, and S. S. P. Parkin, *Phys. Rev. Lett.* **84**, 3462 (2000).
  - <sup>11</sup>R. Schäfer, R. Urban, D. Ullmann, H. L. Meyerheim, B. Heinrich, L. Schultz, and J. Kirschner, *Phys. Rev. B* **65**, 144405 (2002).
  - <sup>12</sup>J. L. Erskine and E. A. Stern, *Phys. Rev. B* **12**, 5016 (1975); G. Schütz, W. Wagner, W. Wilhelm, P. Kienle, R. Zeller, R. Frahm, and G. Materlik, *Phys. Rev. Lett.* **58**, 737 (1987).
  - <sup>13</sup>J. Stöhr, Y. Wu, M. G. Samant, B. B. Hermsmeier, G. Harp, S. Koranda, D. Dunham, and B. P. Tonner, *Science* (Washington, DC, U.S.) **259**, 658 (1993).
  - <sup>14</sup>J. J. de Miguel, A. Cebollada, J. M. Ferrer, R. Miranda, C. M. Schneider, P. Bressler, J. Garbe, K. Bethke, and J. Kirschner, *Surf. Sci.* **211-212**, 732 (1989); C. M. Schneider, P. Bressler, P. Schuster, J. Kirschner, J. J. de Miguel, and R. Miranda, *Phys. Rev. Lett.* **64**, 1059 (1990).
  - <sup>15</sup>P. Krams, F. Lauks, R. L. Stamps, B. Hillebrands, and G. Güntherodt, *Phys. Rev. Lett.* **69**, 3674 (1992).
  - <sup>16</sup>M. Kowalewski, C. M. Schneider, and B. Heinrich, *Phys. Rev. B* **47**, 8748 (1993).
  - <sup>17</sup>W. L. O'Brien and B. P. Tonner, *Phys. Rev. B* **49**, 15 370 (1994).
  - <sup>18</sup>B. Schulz and K. Baberschke, *Phys. Rev. B* **50**, 13 467 (1994).
  - <sup>19</sup>M. Farle, B. Mirwald-Schulz, A. N. Anisimov, W. Platow, and K. Baberschke, *Phys. Rev. B* **55**, 3708 (1997).
  - <sup>20</sup>R. Vollmer, T. Gutjahr-Löser, J. Kirschner, S. van Dijken, and B. Poelsema, *Phys. Rev. B* **60**, 6277 (1999).
  - <sup>21</sup>W. Kuch, Xingyu Gao, and J. Kirschner, *Phys. Rev. B* **65**, 064406 (2002).
  - <sup>22</sup>J. Shen, M.-T. Lin, J. Giergiel, C. Schmidthals, M. Zharnikov, C. M. Schneider, and J. Kirschner, *J. Magn. Magn. Mater.* **156**, 104 (1996).
  - <sup>23</sup>W. Kuch, J. Gilles, F. Offi, S. S. Kang, S. Imada, S. Suga, and J. Kirschner, *J. Electron Spectrosc. Relat. Phenom.* **109**, 249 (2000).
  - <sup>24</sup>W. Kuch, R. Frömter, J. Gilles, D. Hartmann, Ch. Ziethen, C. M. Schneider, G. Schönhense, W. Swiech, and J. Kirschner, *Surf. Rev. Lett.* **5**, 1241 (1998).
  - <sup>25</sup>A. Hubert and R. Schäfer, *Magnetic Domains* (Springer, Berlin, 1998).
  - <sup>26</sup>The simulations were performed using the LLG *Micromagnetic Simulator<sup>TM</sup>* by M. Scheinfein.
  - <sup>27</sup>W. Platow, U. Bovensiepen, P. Pouloupoulos, M. Farle, K. Baberschke, L. Hammer, S. Walter, S. Müller, and K. Heinz, *Phys. Rev. B* **59**, 12 641 (1999).
  - <sup>28</sup>J. R. Cerdá, P. L. de Andres, A. Cebollada, R. Miranda, E. Navas, P. Schuster, C. M. Schneider, and J. Kirschner, *J. Phys.: Condens. Matter* **5**, 2055 (1993).
  - <sup>29</sup>See, for example, Eq. (3.149) of Ref. 25, or A. Thiaville, J. Miltat, and J.-M. García, in *Magnetic Microscopy of Nanostructures*, edited by H. Hopster and H. P. Oepen (Springer, Berlin, in press).
  - <sup>30</sup>B. Heinrich, T. Monchesky, and R. Urban, *J. Magn. Magn. Mater.* **236**, 339 (2001).
  - <sup>31</sup>V. K. Vlasko-Vlasov, U. Welp, J. S. Jiang, D. J. Miller, G. W. Crabtree, and S. D. Bader, *Phys. Rev. Lett.* **86**, 4386 (2001).
  - <sup>32</sup>W. Weber, R. Allenspach, and A. Bischof, *Appl. Phys. Lett.* **70**, 520 (1997).
  - <sup>33</sup>P. J. Jensen, K. H. Bennemann, P. Pouloupoulos, M. Farle, F. Wilhelm, and K. Baberschke, *Phys. Rev. B* **60**, R14 994 (1999).
  - <sup>34</sup>W. Kuch, Xingyu Gao, J. Gilles, and J. Kirschner, *J. Magn. Magn. Mater.* **242-245**, 1246 (2002).
  - <sup>35</sup>M. Speckmann, H. P. Oepen, and H. Ibach, *Phys. Rev. Lett.* **75**, 2035 (1995).
  - <sup>36</sup>K. Fukumoto, H. Daimon, L. Chelaru, F. Offi, W. Kuch, and J. Kirschner, *Surf. Sci.* **514**, 151 (2002).
  - <sup>37</sup>H. P. Oepen, *J. Magn. Magn. Mater.* **93**, 116 (1991).